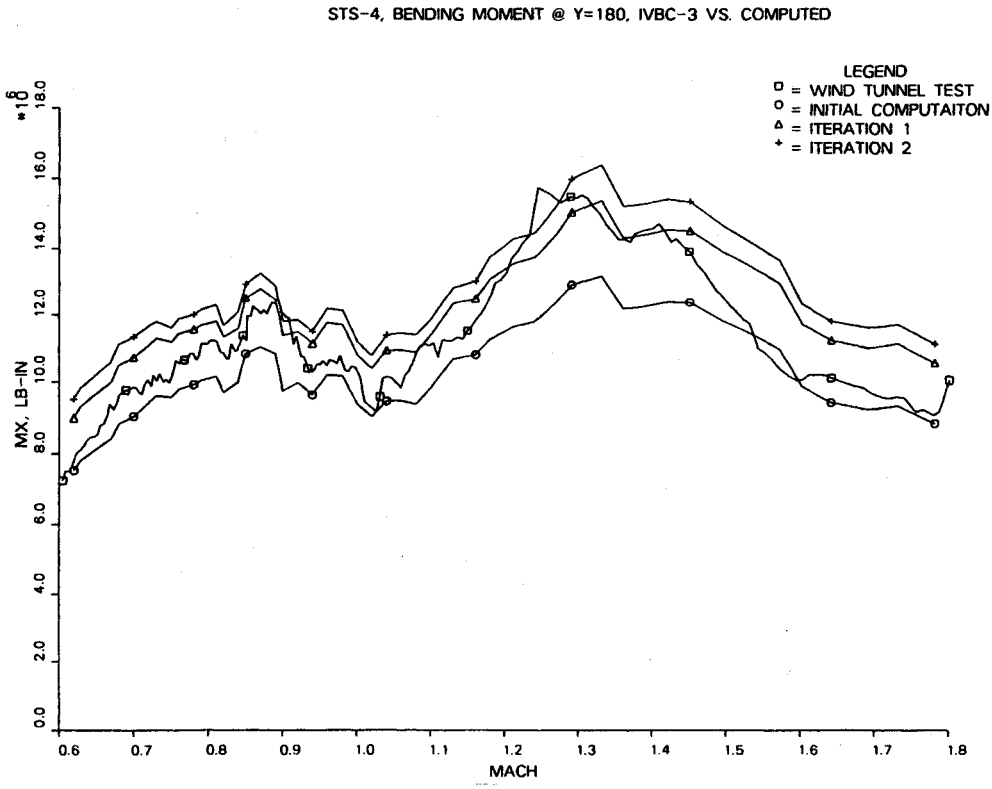

Fig. 3 Comparison of measured and computed bending moment vs Mach number (STS-4, bending moment at y = 180, IVBC-3).

Table 1

Iteration no.	Interpolation polynomial	
	Lift	Drag
0	2nd order	1st order
1	3rd order	2nd order
2	4th order	3rd order

The instrumentation layout (see Fig. 1) shows the coordinates; Sta is the area on wing from station y = 180 in. to tip. The variation in *SZ* and *MX* with Mach number are shown in Figs. 2 and 3, respectively.

Notice that the computed terms *SZ* and *MX* do not directly reflect the influence of drag force on the wing; however, the inclusion of drag terms in the assumed force distribution is necessary to account for drag effects on structural strain as recorded by the strain gauges. In addition to lift and drag distributions, an assumed twisting moment along the leading edge might be used to account for leading-edge suction effects. It was not used in this study.

V. Conclusion

By comparison with the wind-tunnel test-based IVBC-3 data, the proposed algorithm shows good correlation. In the transonic region, the proposed algorithm holds some inherent superiority to wind-tunnel test and computation fluid dynamics method due to the fact that the proposed algorithm is based on structural deformation. Because the general principles involved in deriving the algorithm are valid in most other engineering cases, its potential application should be adaptable to any aircraft loading problem.

References

[1]"B-1 Aircraft No. 2 Airload Survey Program Strain Gauge Calibration," Rockwell International Corp., Los Angeles, CA, Rept. No. AD-b027106L TFD-75-958, 1976.

[2]Schneider, E., "Determination of Aircraft Load with the Aid of Strain Gauges," *Wissenschaftliche Gesellschaft Fuer Luft Und Raumfahrt, Year Book,* DGLR, Bonn, FRG, 1967.

[3]Zienkiewicz, O. C., *The Finite Element Method in Engineering Science,* McGraw-Hill, London, 1971.

[4]Rockwell International Corp., IVBC-3 Data Base (unpublished wind-tunnel data), 1988.

Yaw Damping of Elliptic Bodies at High Angles of Attack

William B. Blake*
Wright Research and Development Center, Wright-Patterson Air Force Base, Ohio
and
Billy P. Barnhart†
Bihrle Applied Research, Inc., Jericho, New York

Introduction

DEPARTURE and spin resistant vehicles are necessary for useful flight at high angles of attack. Forebody vortices in this flight regime can dominate the overall configuration stability and departure susceptibility. Rotary balance testing has been used to further our understanding of these flows[1] and to predict aircraft spin characteristics.[2] Experimental results for a series of bodies have been obtained[3,4] using a rotary balance. Bodies that were undamped in yaw at moderate angles of attack became damped as the angle of attack increased.

Received Dec. 26, 1989; presented as Paper 90-0068 at the AIAA 28th Aerospace Sciences Meeting, Reno, NV, Jan. 8-11, 1990.

*Aerospace Engineer. Member AIAA.
†Chief Engineer. Member AIAA.

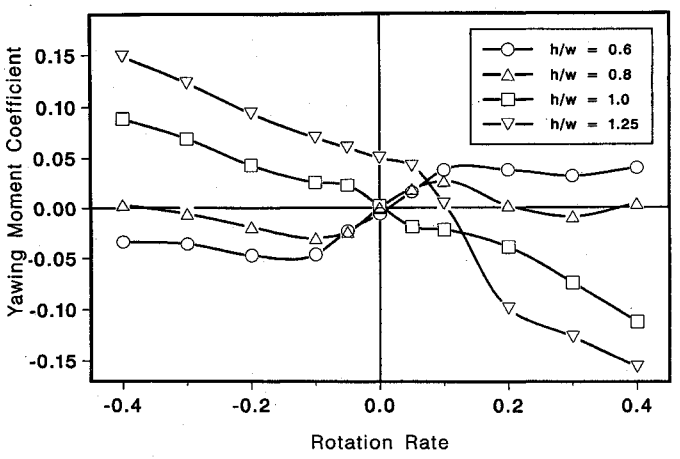

Fig. 1 Effect of body height/width ratio on rotational yawing moment; forebody fineness ratio = 3, angle of attack = 40 deg.

Table 1 Summary of forebody geometries

h/w	l/h (sharp)						l/h (blunt)		
1.25	0.8	1.6	2.4	3.2	3.6	4	2.4	3.2	3.6
1.0	1	2	3	4	4.5	5			
0.8	1	2	3	4	4.5	5	3	4	4.5
0.6	1	2	3	4	4.5	5	3	4	4.5

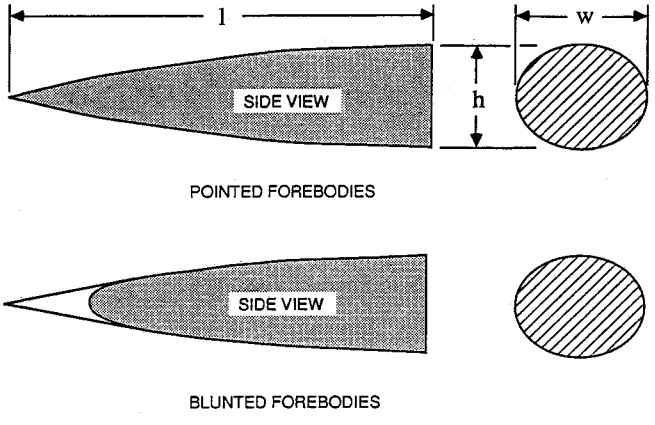

Static trim points encountered during this transition. This Note will present a correlation of these trim points.

Discussion

The test was conducted in the NASA Langley Vertical Wind Tunnel using the rotary balance. The forebody geometries tested are shown in Table 1. All forebodies had a base area of 4π in.^{2}. They were mounted on 49-in.-long afterbodies of the same ellipticity, with the center of rotation 30 in. from the afterbody base. Selected bodies were also tested with a typical wing and vertical tail to determine their influence while in the presence of other aircraft components. The yawing moment coefficients presented here were nondimensionalized by the span and area of the typical wing used during part of the test program (2.8 ft and 3.09 ft^2, respectively). Consistent with Bihrle et al.,[4] body axis yawing moment data will be presented even though the rotary rig generates a wind axis rotation. "Damped in yaw" will be defined as a body axis yawing moment that opposes the wind axis rotation (negative slope of the C_n vs $\Omega b/2V$ curve). The underlined bodies shown in Table 1 were undamped in yaw at moderate angles of attack.

Yawing moments measured at 40-deg angle of attack for the fineness-ratio-3 (3.2 for the h/w 1.25 body) pointed forebodies are shown in Fig. 1. These moments are presented as a function of the dimensionless rotation rate $\Omega b/2V$. For a clockwise rotation ($\Omega b/2V > 0$), positive yawing moments are autorotative (propelling rather than damping), whereas negative moments are damping. A clear effect of ellipticity on yaw damping is evident. The circular and vertically elliptic bodies are damped in yaw, whereas the horizontally elliptic bodies ($h/w < 1.0$) are propelling. The vertically elliptic body exhibits a large static yawing moment offset.

The effect of angle of attack on the 0.6 h/w fineness-ratio-3 forebody is shown in Fig. 2. At the lowest angle of attack (40 deg), the body is completely autorotative. At 50- and 60-deg angle of attack, the body is still undamped, but static trim points ($C_n = 0$ with $\Omega \neq 0$) are observed at the higher rotation rates. At 70-deg angle of attack, the body is completely damped. Similar trends were found for all of the underlined configurations shown in Table 1. Bodies that were undamped in yaw at moderate angles of attack became damped with increasing angle of attack, with a series of static trim points encountered during the transition.

For each undamped body, the data base was canvassed to find the static trim points. Because static yawing moment offsets may influence the rotation rate for static trim, the following method was used to reduce their effects. At each tested rotation rate ($\Omega b/2V$), static trim points were extracted from the data by linearly interpolating between the angles of attack bracketing the following condition:

$$C_n(+\Omega b/2V) - C_n(-\Omega b/2V) = 0 \qquad (1)$$

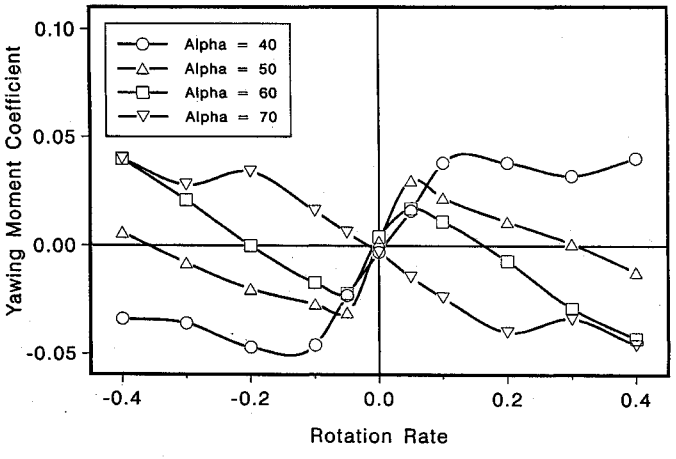

Fig. 2 Effect of angle of attack on rotational yawing moment; forebody fineness ratio = 3, body height/width = 0.6.

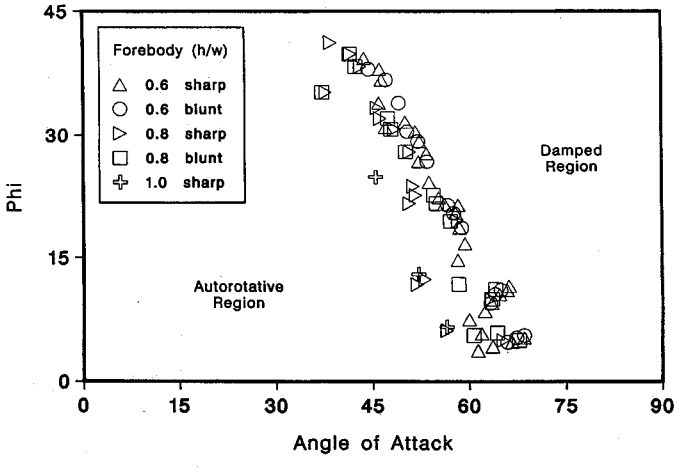

Fig. 3 Static trim boundary for elliptic bodies as a function of angle of attack and effective roll angle.

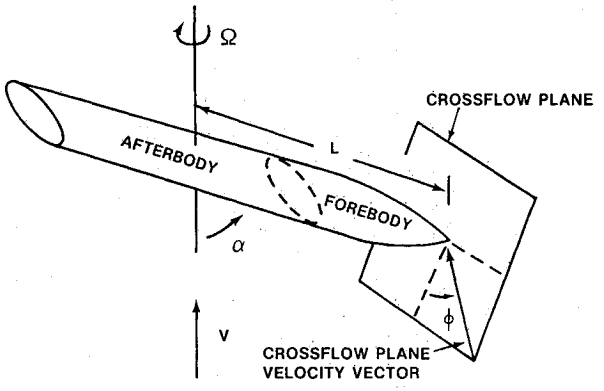

Fig. 4 Definition of effective roll angle.

For example, consider the data shown in Fig. 2 with a rotation rate of 0.4. Equation (1) gives $\Delta C_n = 0.074$ for $\alpha = 40$ deg and -0.018 for $\alpha = 50$ deg. At $\alpha = 45$ deg (the data are not shown for clarity), $\Delta C_n = 0.005$. Interpolation gives 46.1 deg as the angle of attack for static trim.

The static trim data were plotted (see Fig. 3) using as a correlating parameter the effective roll angle ϕ introduced by the rotation. This angle, measured in the crossflow plane at the nose apex (see Fig. 4) is expressed as:

$$\phi = \tan^{-1}[(\Omega L \sin\alpha)/(V \sin\alpha)] = \tan^{-1}[(\Omega b/2V)(2L/b)] \quad (2)$$

The utility of this angle for rotational flow studies was confirmed by Tobak et al.[5] Since the nondimensional rotation rate $\Omega b/2V$ represents the tangent of the helix angle of the wing tip, Eq. (2) represents a correction on $\Omega b/2V$ to the nose apex. Except for some scatter near zero effective roll angle, a linear relationship is clearly indicated in Fig. 3. Some of the 0.8 and 1.0 h/w sharp nose data are shifted slightly to the left of the bulk of the data. It is not known why this is the case.

Two primary flow mechanisms induce aerodynamic yawing moments on bodies under rotational flow conditions. First is the crossflow drag contribution, which, integrated across the entire body, will always be damping. Additional loads are induced by the flow separation with associated vortices shed by the body. These vortices form distinct flow patterns as angle of attack increases. At large angles of attack, the flow separation and associated vortices are asymmetric and induce large side loads and moments. Presumably, the vortex asymmetry is of differing orientation for the damped and undamped bodies at moderate angles of attack. This is consistent with static directional stability and flow visualization findings.[4,7] Autorotative bodies are statically stable whereas damped bodies are statically unstable. As the angle of attack becomes very large ($\alpha = 70$), the body vortices are of the unsteady Karman type, producing no net side force.[6] With no vortex-induced side force to cancel the crossflow drag contribution, there can be no static trim points above this angle of attack. This is what is observed in Fig. 3. Figure 3 is also in qualitative agreement with coning results presented by Yoshinaga et al.[8] For cone-cylinder configurations, they found the steady coning rate decreased with increasing angle of attack with no steady coning found above 65-deg angle of attack.

An airplane's inertial yawing moments in a spin are small relative to the possible aerodynamic moments. Hence, the static trim boundary gives a first-order approximation to where an airplane might spin at any angle of attack. This assumes that the other moments are in equilibrium at that angle of attack and rotation rate and that, in this case, the body's yaw contribution is dominant.

Conclusion

Rotary balance yawing moment data obtained on a series of body-alone configurations have been studied. Reductions in body ellipticity (h/w) decrease yaw damping. Bodies which are undamped at moderate angles of attack become damped as angle of attack increases. Points of static trim in yaw for these bodies ($C_n = 0$ with $\Omega \neq 0$) were found to be linearly related to the effective roll angle introduced by the rotation.

References

[1]Tuttle, M. H., Kilgore, R. A., and Sych, K. L., "Rotary Balances—A Selected, Annotated Bibliography," NASA TM-4150, March 1989.

[2]Bihrle, W., Jr., and Barnhart, B., "Spin Prediction Techniques," *Journal of Aircraft*, Vol. 20, No. 2, 1983, pp. 97–101.

[3]Bihrle, W., Jr., Barnhart, B., and Dickes, E., "Static and Rotational Aerodynamic Data from 0° to 90° Angle of Attack for a Series of Basic and Altered Forebody Shapes," Wright Research and Development Center, WPAFS, OH, TR-89-3090, Sept. 1989.

[4]Bihrle, W., Jr., Barnhart, B., and Dickes, E., "Influence of Forebody Geometry on Aerodynamic Characteristics and a Design Guide for Defining Departure/Spin Resistant Forebody Configurations," Wright Research and Development Center, WPAFS, OH, TR-89-3079, Sept. 1989.

[5]Tobak, M., Schiff, L. B., and Peterson, V. L., "Aerodynamics of Bodies of Revolution in Coning Motion," *AIAA Journal*, Vol. 7, No. 1, 1969, pp. 96–99.

[6]Ericsson, L. E., "Reflections Regarding Recent Rotary Rig Results," *Journal of Aircraft*, Vol. 24, No. 1, 1987, pp. 25–30.

[7]Brandon, J. M., and Nguyen, L. T., "Experimental Study of Effects of Forebody Geometry on High Angle-of-Attack Stability," *Journal of Aircraft*, Vol. 25, No. 7, 1988, pp. 591–597.

[8]Yoshinaga, T., Tate, A., and Inoue, K., "Coning Motion of Slender Bodies at High Angles of Attack in Low Speed Flow," AIAA Paper 81-1899, Aug. 1981.